AGU PUBLICATIONS

JGR

Journal of Geophysical Research: Atmospheres

RESEARCH ARTICLE
10.1002/2017JD026597

Key Points:
- Rossby wave generation events in the middle atmosphere are classified statistically using an automatic detection technique
- The eastward forcing due to Rossby wave generation dominates Eliassen-Palm flux divergence in the winter polar stratopause
- he mean duration of the Rossby wave generation events is of 3.35 day and about 24 events a year are found

Correspondence to:
M. Pulido,
pulido@unne.edu.ar

Citation:
Rodas, C., and M. Pulido (2017), A climatology of Rossby wave generation in the middle atmosphere of the Southern hemisphere from MERRA reanalysis, *J. Geophys. Res. Atmos.*, *122*, 8982–8997, doi:10.1002/2017JD026597.

Received 6 FEB 2017
Accepted 17 JUL 2017
Accepted article online 21 JUL 2017
Published online 3 SEP 2017

A climatology of Rossby wave generation in the middle atmosphere of the Southern Hemisphere from MERRA reanalysis

Claudio Rodas[1] **and Manuel Pulido**[1,2]

[1]Department of Physics, FACENA, Universidad Nacional del Nordeste, Corrientes, Argentina, [2]IFAECI UMI-CNRS and IMIT, CONICET, Corrientes, Argentina

Abstract A climatological characterization of Rossby wave generation events in the middle atmosphere of the Southern Hemisphere is conducted using 20 years of Modern-Era Retrospective Analysis for Research and Applications (MERRA) reanalysis. An automatic detection technique of wave generation events is developed and applied to MERRA reanalysis. The Rossby wave generation events with wave period of 1.25 to 5.5 days and zonal wave number from one to three dominate the Eliassen-Palm flux divergence around the stratopause at high latitudes in the examined 20 year period. These produce an eastward forcing of the general circulation between May and mid-August in that region. Afterward from mid-August to the final warming date, Rossby wave generation events are still present but the Eliassen-Palm flux divergence in the polar stratopause is dominated by low-frequency Rossby waves that propagate from the troposphere. The Rossby wave generation events are associated with potential vorticity gradient inversion, and so they are a manifestation of the dominant barotropic/baroclinic unstable modes that grow at the cost of smearing the negative meridional gradient of potential vorticity. The most likely region of wave generation is found between 60° and 80°S and at a height of 0.7 hPa, but events were detected from 40 hPa to 0.3 hPa (which is the top of the examined region). The mean number of events per year is 24, and its mean duration is 3.35 days. The event duration follows an exponential distribution.

Plain Language Summary A climatological characterization of Rossby wave generation events in the middle atmosphere of the Southern Hemisphere is conducted using 20 years of MERRA reanalysis. Rossby wave generation events in the middle atmosphere are classified statistically using an automatic detection technique. The eastward forcing due to Rossby wave generation dominates Eliassen-Palm flux divergence in the winter polar stratopause. The mean duration of the Rossby wave generation events is 3.35 days and about 24 events a year are found. We conclude that the middle atmosphere is a very active region that generates internally a rich spectrum of midfrequency Rossby waves. These waves dominate the Eliassen-Palm flux divergence at high latitudes of the Southern Hemisphere during a large part of the austral winter.

1. Introduction

Most of the middle atmosphere dynamical variability is thought to be dominated by large-scale waves that originate in the troposphere, propagate upward, and then break in the middle atmosphere. As long as the waves propagate conservatively upward, they produce only reversible effects on the general circulation. When the wave disturbance has passed through the region, the mean flow recovers its original state [*Andrews and McIntyre*, 1978]. During its propagation, Rossby waves are refracted by the mean flow so that the path followed by Eliassen-Palm flux is traced primarily by the zonal wind through the refraction index [*Charney and Drazin*, 1961]. In the regions where waves break or dissipate, they produce permanent changes in the general circulation. The zonal-phase propagation of Rossby waves is westward with respect to the local zonal wind, so that the breaking of Rossby waves is expected to decelerate the strong westerly zonal wind that prevails in the winter stratosphere. In other words, the breaking of Rossby waves produces a nonreversible westward zonal forcing on the general circulation, which is determined from the Eliassen-Palm flux divergence.

Figure 1 shows the 20 year mean zonally averaged Eliassen-Palm flux divergence (EPFD) determined from Modern-Era Retrospective Analysis for Research and Applications (MERRA) reanalysis for July. Most of the

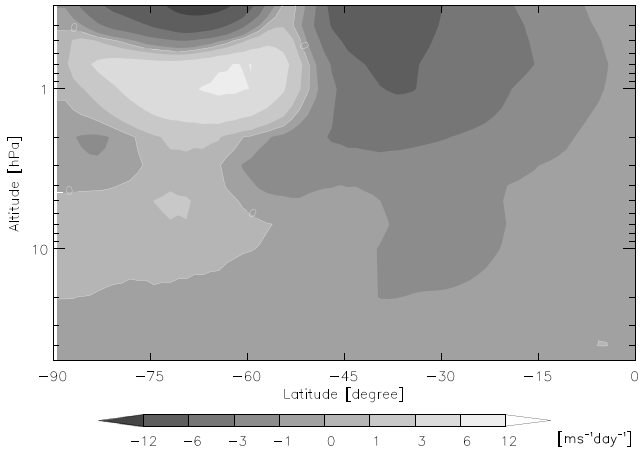

Figure 1. EPFD for July averaged between 1991 and 2010 from MERRA reanalysis data. Light gray shading represents eastward forcing. The white line denotes the zero contour.

stratosphere is dominated by a negative pattern which is reminiscent of Rossby wave breaking and dissipation. Planetary waves are generated in the troposphere, they propagate upward on the westerly zonal winds during winter and dissipate in the middle atmosphere producing a westward forcing to the zonal mean flow. The midlatitude forcing produced by planetary waves is the main mechanism responsible of the Brewer-Dowson circulation which advects air from the equatorial tropopause toward the stratosphere at midlatitudes [*Butchart*, 2014]. A large eastward EPFD pattern in Figure 1 is clearly visible at southern high latitudes centered at the stratopause but extending toward lower and higher altitudes. This pattern can only be associated with local Rossby wave generation. It is present in a 20 year mean and it can be found as low as 10 hPa in July in high latitudes of the Southern Hemisphere. This is a rather important feature showing that barotropic and/or baroclinic instability and its concomitant Rossby wave generation in the middle atmosphere has a nonnegligible climatological impact on the middle atmosphere general circulation, so that it deserves further research and motivates this work.

The possibility that the middle atmosphere could be not only a passive receiver of disturbances from the lower atmosphere but also a source of them, was earlier raised in *Charney and Stern* [1962]. At the stratopause close to the annular boundary of the winter polar darkness, a sharp meridional temperature gradient is established every year which implies a sharp and strong zonal jet. At the flanks of this jet, a negative potential vorticity gradient is expected if the zonal wind meridional curvature of the jet is large enough. This is a necessary condition for the development of barotropic instabilities which are a source of planetary-scale waves. *Hartmann* [1983] found that unstable barotropic modes associated with the regions of negative potential vorticity gradient on the polar flank of the jet have significant growth rates. The most unstable modes have wave numbers 1 and 2 and periods of 3–4 days and 1.5–2 days, respectively. On the equatorward flank of the jet, he found that waves with wave numbers 1 to 3 are most unstable and they have periods much longer, from 1 to 3 weeks. *Manney and Randel* [1993] evaluated the role of barotropic and baroclinic components of the instability during Rossby wave generation at the stratopause. They concluded that both components are required to give realistic growth rates.

Venne and Stanford [1979] presented the first observational evidence from Nimbus 4 and 5 measurements of a 4 day wave propagating eastward. The oscillation was found at the polar winter stratosphere in both hemispheres, but with stronger amplitudes in the Southern Hemisphere. Subsequently, *Prata* [1984] using Nimbus 5 and 6 found evidence of an event of a disturbance with two components: a wave number 1 with a 4 day period, and a wave number 2 oscillation with a 2 day period, which propagate eastward and were observed together. That work associated the event with a "warm pool" circling the pole with a period of near 4 days. The warm pool retains its identity several complete revolutions around the pole [*Prata*, 1984]. This warm pool may be composed of ground-based eastward propagating waves with zonal wave numbers 1, 2, or even higher. The higher zonal wave number components have the higher frequencies, such that all components propagate with the same phase speed. This unique phase speed of the wave event is a manifestation of a nondispersive wave disturbance, and because of that it can be observed for several days. Furthermore, this is a manifestation that all the waves were produced by the same instability event so that the phase speed of the waves is related to the mean zonal flow found at the place of the instability. *Manney* [1991] examined stratospheric 4 day wave events based on 10 years of the National Meteorological Center geopotential height data. A spectral analysis of the wave number 1 component was conducted at 10 and 2 hPa. She finds two distinct types of patterns related to the wave events. One in which the amplitude has a single high-latitude maximum and the other with two maxima at different latitudes. The latter was associated with the double-jet

structure of the winter mesosphere. *Coy et al.* [2003] examined 4 day wave events in Goddard Space Flight Center meteorological and ozone analysis. They show that the events affect the transport and distribution of ozone. Indeed, a clear signature of the wave event is found in the Polar Ozone and Aerosol Measurement (POAM) ozone data in good agreement with analysis data.

Evidence of the 4 day wave has also been reported in the Antarctic upper mesosphere, *Lawrence et al.* [1995] found that the 4 day wave was detected through radar wind observations in the upper mesosphere up to 90 km in coherence with the presence of this wave in stratospheric analyses. Because of its nondispersive nature (and wave amplitude increase due to density decrease), the wave phenomenon can be detected several scale heights above its generation altitude. *Lawrence and Randel* [1996] also found in Nimbus 6 data a 4 day wave event that generates at the stratopause and extends up to the upper mesosphere. They show that 4 day peaks are also detected in the Northern Hemisphere in November of each year, but they are much weaker. *Garcia et al.* [2005] show evidence of a 4 day wave during boreal winter in Sounding of the Atmosphere using Broadband Emission Radiometry (SABER) observations which also extends up to the mesosphere. The phase of the wave remains nearly constant and a 180° phase jump is found at 60 km consistent with the structure expected from linear baroclinic instability [*Manney and Randel*, 1993].

Watanabe et al. [2009] show that the processes related to the generation of 4 day waves has an important role in the budget of the upper stratosphere and the lower mesosphere. Using a relatively high vertical resolution general circulation model that directly simulates the spontaneous generation, propagation, and dissipation of gravity waves, they found that the simulated 4 day waves develop in baroclinically and barotropically unstable flows. Events associated with a single- and double-jet structure with very strong eastward forcing exceeding 10 m s^{-1} d^{-1} were found in the simulations.

Here we examine Rossby wave generation in the upper stratosphere of the Southern Hemisphere from 1991 to 2010 using MERRA reanalysis data. We focus on the Southern Hemisphere middle atmosphere because the barotropic-baroclinic instability is expected to be stronger there, than in the Northern Hemisphere middle atmosphere, where the polar winter jet and its horizontal and vertical curvatures are substantially weaker [*Lawrence and Randel*, 1996]. Aspects of the data and methodology are described in section 2. A general spectral analysis of the generated waves in the 20 years is produced (section 3.1). The Eliassen-Palm fluxes and the EPFD field associated with the locally generated Rossby waves are isolated and examined. Two paradigmatic case studies found in the reanalysis data are examined (section 3.2), one in the poleward flank and the other one in the equatorward flanks of the stratospheric jet. In this work, we establish a set of criteria to detect automatically Rossby wave generation events in the middle atmosphere. The detection criteria are applied to the 20 year MERRA reanalysis data. We then produce a statistical characterization of the events (section 3.3). Several climatological aspects of the instability events are characterized on a multiyear analysis: the frequency of the events, the time length of the events, preferred locations and time of the year, and their effects on the general circulation of the middle atmosphere. Conclusions are drawn in section 4.

2. Methodology

2.1. Rossby Wave Flux and Forcing

The most convenient framework to examine the forcing of the zonal-mean circulation by waves is through the transformed Eulerian mean equations [*Andrews et al.*, 1987, pg. 128]. The log pressure is taken as the vertical coordinate

$$z_p = -H \ln(p/p_s), \tag{1}$$

where p_s is a reference pressure.

The horizontal component of the transformed Eulerian mean meridional circulation is defined by

$$v^* = \overline{v} - \rho_0^{-1} \partial_{z_p} \left(\rho_0 \overline{\theta}_z^{-1} \overline{v'\theta'} \right), \tag{2}$$

and the vertical component of the transformed Eulerian mean meridional circulation by

$$w^* = \overline{w} + (a \cos\phi)^{-1} \partial_\phi \left(\cos\phi \overline{\theta}_z^{-1} \overline{v'\theta'} \right), \tag{3}$$

where a is the mean Earth radius, ρ_0 is the basic state density, ϕ is latitude, θ is the potential temperature, and $\overline{\theta}_z = \partial_{z_p}\overline{\theta}$. Zonal-mean fields are denoted by an overbar and perturbations to them are denoted by a prime. With this transformation, the only forcing term that affects the zonal wind equation from resolved eddies is the divergence of the Eliassen-Palm flux.

The meridional Eliassen-Palm flux is defined as

$$F_\phi = \rho_0 a \cos\phi \left(\overline{u}_z \overline{\theta}_z^{-1} \overline{v'\theta'} - \overline{u'v'} \right), \tag{4}$$

where $\rho_0 = \frac{p}{Hg}$. The vertical Eliassen-Palm flux is

$$F_{z_p} = \rho_0 a \cos\phi \left\{ \left[f - (a\cos\phi)^{-1} \left(\overline{u}\cos\phi \right)_\phi \right] \overline{\theta}_z^{-1} \overline{v'\theta'} - \overline{u'w'} \right\}. \tag{5}$$

The zonal-mean acceleration which forces the transformed Eulerian mean zonal wind equation in this formulation is produced by the divergence of the Eliassen-Palm flux, which taking the divergence from (4) and (5) is given by

$$\overline{X} = (\rho_0 a \cos\phi)^{-1} \left[(a\cos\phi)^{-1} \partial_\phi \left(F_\phi \cos\phi \right) + \partial_{z_p} F_{z_p} \right]. \tag{6}$$

In this work, we refer to $\overline{X}$ in (6) as EPFD (Eliassen-Palm Flux Divergence). The resulting transformed Eulerian mean zonal wind equation is

$$\partial_t \overline{u} + v^* \left[-f + (a\cos\phi)^{-1} \partial_\phi \left(\overline{u}\cos\phi \right) \right] + w^* \partial_{z_p} \overline{u} = \overline{X} + \overline{X}_{\mathrm{GW}}, \tag{7}$$

where $\overline{X}_{\mathrm{GW}}$ represents the forcing by unresolved waves in the model, i.e., waves that are not considered in the eddy quantities, u', w', in particular, small-scale unresolved gravity waves.

In an equilibrium state, we can think of the zonal-forcing term (6) as the main driver of the residual mean meridional circulation in the lower stratosphere. In other words, a quasi-steady forcing is mainly compensated with the Coriolis term of the residual mean meridional circulation in (7), while the continuity equation relates the residual mean meridional circulation to the residual mean vertical circulation at the sides of the forcing region. In the case of a sudden forcing, the EPFD produces an acceleration and it also drives the meridional circulation [*Garcia*, 1987]. In the middle stratosphere, both forcing terms $\overline{X}$ and $\overline{X}_{\mathrm{GW}}$ are nonnegligible and contribute to produce the residual mean meridional circulation. The $\overline{X}$ forcing at these heights is expected to be larger during boreal winter, but smaller during austral winter. In the upper stratosphere and lower mesosphere, we expect that the forcing by gravity waves $\overline{X}_{\mathrm{GW}}$ dominates the residual mean meridional circulation. An estimation of this forcing term, $\overline{X}_{\mathrm{GW}}$, in the middle atmosphere from reanalyses was produced in *Pulido and Thuburn* [2006, 2008]. A useful framework to readily determine $\overline{X}_{\mathrm{GW}}$ is from potential vorticity budget [*Pulido*, 2014].

2.2. Data Treatment

In this work, the NASA's Modern-Era Retrospective Analysis for Research and Applications (MERRA) are used from year 1991 to 2010. The data are available in a horizontal resolution of 1.25° and in 42 vertical levels up to a height of 0.1 hPa. The assimilation system is based on the GEOS-5 atmospheric general circulation model. The assimilation system uses a three-dimensional variational data assimilation technique. The analysis innovations are determined through the incremental analysis update approach. In this approach, the corrections to the model state are introduced through forcing terms along the assimilation cycles so that the model evolves smoothly and it is not reset every assimilation cycle as in other assimilation techniques. This approach avoids model spin-up. Therefore, these reanalysis data appear particularly suitable for budget studies. More details of the assimilation system are available in *Rienecker et al.* [2011].

To our knowledge, there is at least an earlier work that examines a 4 day wave event from MERRA reanalysis [*Lu et al.*, 2013]. They found good agreement between reanalysis and lidar data. *Coy et al.* [2003] used an earlier version of the NASA's data assimilation system, and they also found good agreement between analysis 4 day wave events and ozone observations from POAM.

MERRA reanalysis has the typical time resolution of current assimilation systems of 6 h, which can capture adequately the 2 day component of the events. Some amplitude of the components of the events with positive zonal wave numbers 3 and 4 is also captured (with a period of about 1.2 days and 0.9 day), but these components are expected to be affected by the temporal resolution of the data.

The internally generated planetary waves are expected to propagate up to the upper mesosphere and lower thermosphere [*Garcia et al.*, 2005; *Chandran et al.*, 2013; *Sassi and Liu*, 2014]; however, the MERRA reanalysis is available up to 0.1 hPa (while GEOS-5 model reaches 0.01 hPa). We also note that the highest levels of MERRA reanalysis are less constrained from observations (channel 14 of the Advanced Microwave Sounding Unit (AMSU) peaks at 1 hPa [*Polavarapu and Pulido*, 2017]). However, these heights are partially constrained by observational information propagating upward in the assimilation system. In this sense, *Nezlin et al.* [2009] showed that the mesospheric large-scale dynamics in the analysis of an assimilation system is constrained by observations taken below 1 hPa. Since the top of the GEOS-5 model is at 0.01 hPa, we also expect that the highest model layers are influenced by the sponge layer, which tends to dissipate waves. Therefore, we focus our analysis at heights lower than 0.3 hPa. From a preliminary general analysis (e.g., Figure 1), we determine that the pressure range for probable Rossby wave generation in MERRA reanalysis is between 10 hPa and 0.3 hPa. The highest number of cases is found at 0.7 hPa. The largest amplitudes are found at 1 hPa.

A spectral analysis of the data is conducted. For each height and latitude, the two-dimensional Fourier spectrum of the disturbance in zonal wave number and frequency is calculated. We took all the longitudinal points (288 points), and for convenience of the Fourier analysis routines (fast Fourier transform), we took 1024 temporal data points each year, from 11 March to 20 November. This period covers the whole life cycle of the stratospheric winter jet in the Southern Hemisphere, in which we expect the instability events. In the frequency-wave number space, we kept only the wave components that propagate eastward. To these Fourier components, a band-pass filter which spans frequencies ranging from 1.25 to 5.5 days and wave numbers from 1 to 3 is applied. The filter used is nonrecursive, and a Kaiser window is applied to avoid Gibbs effects (see *Scavuzzo et al.* [1998] for details). The Nyquist period for the data is 0.5 day. To determine the contribution of the 4 day waves to the EPFD, the inverse Fourier transform is applied to the resulting filtered Fourier fields needed to determine $\overline{X}$ from (6).

In principle, there are two latitudinal bands in which we expect Rossby wave generation events: the poleward flank and the equatorward flank of the stratospheric jet. For the poleward flank, we take as reference latitudinal band 65°–75°S; while for the equatorward flank it is not possible to define a reference latitudinal band. It has large latitudinal variability, and much fewer cases are detected than in the poleward flank. Since we have limited the period range from 1.25 to 5.5 days, some of the equatorward flank events may be filtered. We use a conservative (narrow) period range to avoid contamination of waves from other sources.

2.3. Automatic Event Detection

This work examines the climatological characteristics of barotropic/baroclinic instabilities in the stratospheric nocturnal jet and its subsequent Rossby wave generation using 20 year reanalysis data. To classify statistically the events, we developed an automatic technique that determines the occurrence of wave generation and the location where it occurs. We take the filtered EPFD field as the most relevant indicator of the effects of Rossby wave generation in the middle atmosphere circulation. The detection technique is applied to it. To avoid a noisy field, we first conduct a running 5 day time average window to the filtered EPFD field. This running window removes noisy peaks and transient features.

Local maximal points in the EPFD field that satisfy $\overline{X} > 2.5$ m s^{-1} d^{-1} at a time frame are preselected. The nearest neighbor points in the grid to the preselected local maximum are also required to have $\overline{X} > 2.5$ m s^{-1} d^{-1}. The position of the local maximum that satisfies the criteria is selected as a potential instability location. The acceleration threshold of 2.5 m s^{-1} d^{-1} was chosen after preliminary experiments and some direct inspection of the events. If another local maximum is found in the neighborhood of a local maximum (5 km in height and 5° in latitude), we assume that the two maxima belong to the same event and an average position is assigned to the event. For the subsequent time frame, again the local maximum points are searched and selected. If one of the selected points is close enough to one of the points selected in the previous frame, we consider this to be a continuation of the same event. If there is no close local maximum point in the previous frame, it is considered as a new possible event. We require a minimum of four time frames (1 day) to be considered as a generation event. This requirement is important to eliminate transient features which are

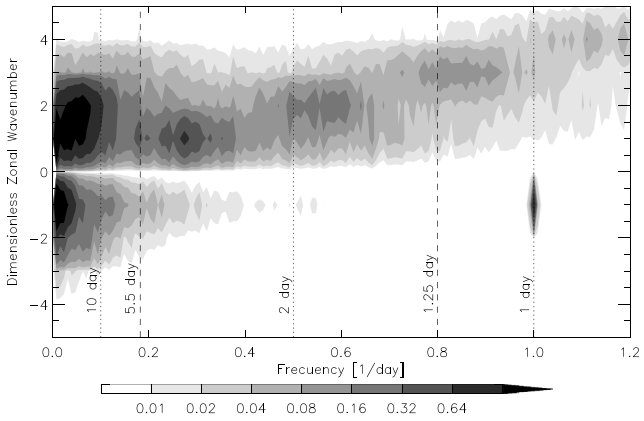

Figure 2. Power spectrum density as a function of wave number and frequency for the zonal wind perturbation at a height of 0.70 hPa and at a latitudinal band of 65°–75°S averaged for 1991–2010. Vertical dashed lines show the 1.25–5.5 day period range that is used in the filter. For reference, the 1, 2, and 10 day periods are shown with vertical dotted lines. The positive zonal wave numbers represent waves with eastward ground-based phase speed.

not associated with Rossby wave generation and also features relatively close to the center of an evolving instability event which do not persist in time.

3. Results

3.1. Main Features

Figure 2 shows the 20 year averaged power spectrum density for the zonal wind perturbation at a height of 0.70 hPa and at a latitudinal band of 65°–75°S. The spectrum is dominated by waves with low (1–5) zonal wave numbers for frequencies higher than 1.2day^{-1}. There are large amplitudes at the lower frequency components (with periods longer than 10 days). The positive zonal wave number part of the spectrum represents waves that propagate eastward relative to a ground-based reference frame. For these waves, there is a clear peak around wave number 1 and at a frequency of 0.27 day^{-1}. A more extended peak at zonal wave number 2, in a range of frequencies from 0.5 to 0.6 day^{-1}, is also present in Figure 2. A third peak is found for a zonal wave number of 3 at 0.70 hPa, with a frequency range that covers from 0.75 to 0.97 day^{-1}. Finally, a fourth peak in zonal wave number 4 with smaller amplitude appears around 1.1 day^{-1}. The zonal wave numbers and frequencies of these four peaks coincide roughly with the ones expected from the barotropic instability growth analysis [e.g., *Hartmann*, 1983]. Besides, the peaks at wave numbers 1–4 and frequencies of 0.27 to 1.1 day^{-1} define a line of constant phase speed of about ≈40 m/s at 70° (which is coherent with the 4 day wave, i.e., the wave with this ground-based phase speed takes 4 days to circle the pole). The sharp peak at wave number −1 and 1 day period can be attributed to the diurnal tide. We focus in this work on the period range of 1.25 days to 5.5 days where the wave numbers 1 and 2 peaks associated with barotropic instability are found.

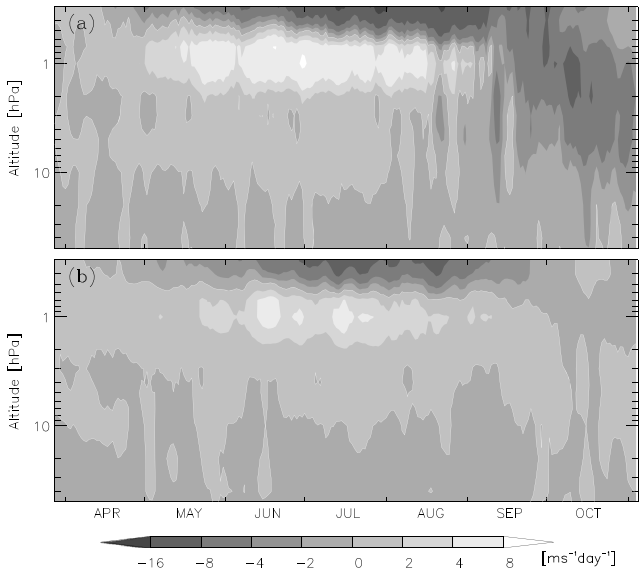

Figure 3. EPFD as a function of time and height in the latitudinal band of 65°–75°S averaged for 1991–2010. (a) EPFD from the total perturbation fields. (b) EPFD from the filtered perturbation fields. The white line denotes the zero contour.

The EPFD averaged in the latitudinal band of 65°–75°S is shown in Figure 3a. From May to August, the eastward forcing center prevails in this latitudinal band. It reaches down to 10 hPa, particularly during June and July. Figure 3b depicts the contribution of the period 1.25–5.5 days and wave numbers 1–3 spectral components to the EPFD. The positive center is well represented by these components. The amplitude is about 2 m s^{-1} d^{-1} weaker that the entire field. This difference is expected to be produced by higher and lower frequency 1–5 wave number waves. The contribution to EPFD of higher (than 5) wave number waves to the positive center is practically negligible in MERRA data. Above the positive center, a rather strong deceleration region ≈10 m s^{-1} d^{-1} exists produced by the 1.25–5.5 day spectral band. A large portion of this deceleration center is likely produced by waves that are generated in

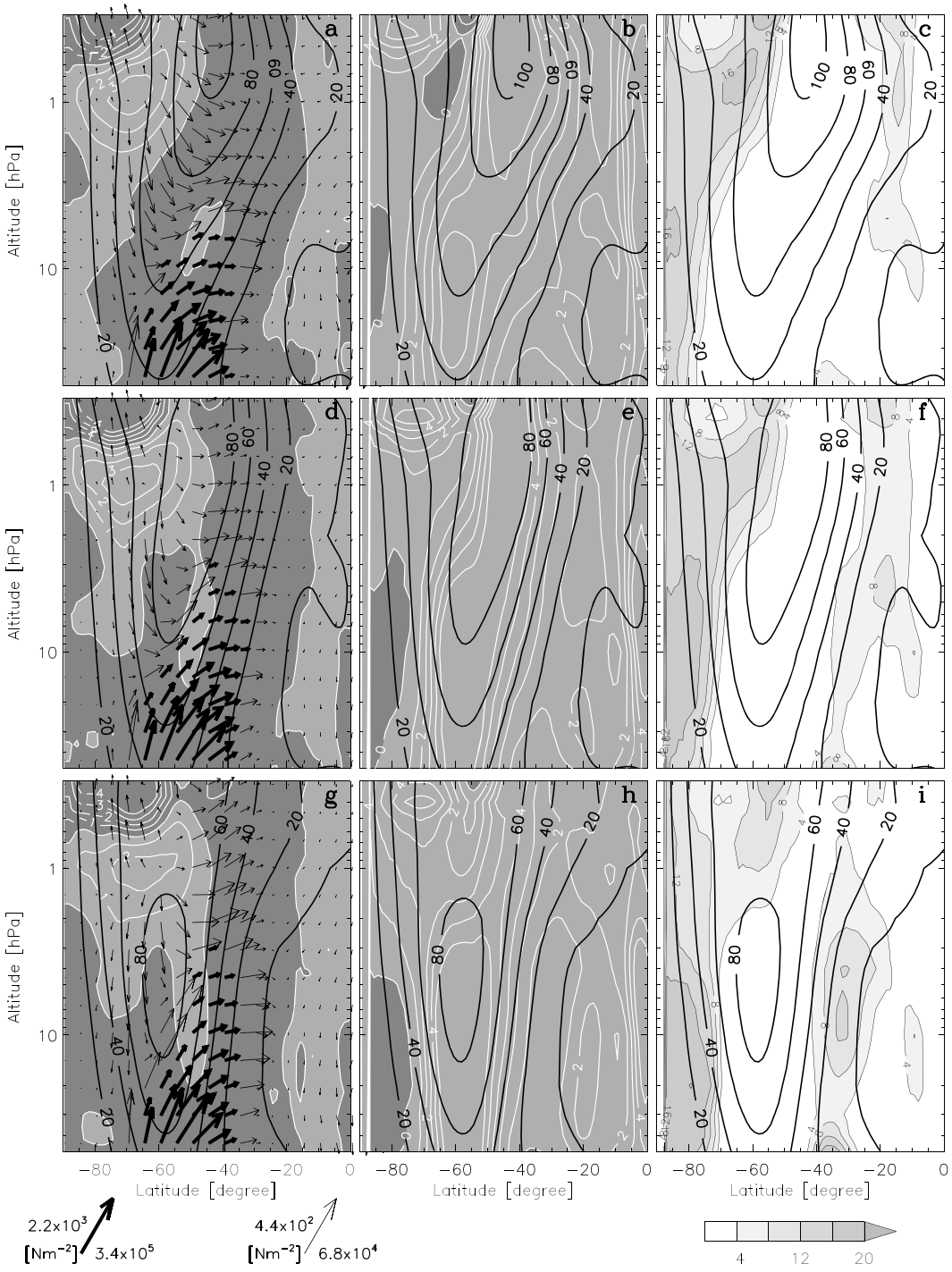

Figure 4. Monthly mean EPFD and the Eliassen-Palm flux (vectors) averaged for 1991–2010 for (a) June, (d) July, and (g) August. Light (dark) gray shading represents positive (negative) EPFD. Meridional gradient of potential vorticity for (b) June, (e) July, and (h) August. Dark gray shading represents negative meridional gradient. Number of days in the corresponding month for which an inversion of potential vorticity latitudinal gradient arises for (c) June, (f) July, and (i) August. The zonal-mean zonal wind is also shown for reference (black contours). Note that vectors have two scales.

the positive center. On the other hand, most of the negative EPFD peaks that arise between 10 and 3 hPa in August and subsequent months which are present in Figure 3a but not in Figure 3b are produced by very low frequency waves (with periods longer than 5.5 days). These include the negative-forcing patterns found in October that produce the final warming and its concomitant vortex breakdown.

Figure 4 depicts the 20 year monthly mean EPFD for the winter months ((a) June, (d) July, and (g) August). In terms of magnitude, June and July are the months that show the strongest eastward forcing around 1 hPa. The equatorward flank is weak in June and then intensifies for July and August. The Eliassen-Palm flux is dominated in the lower stratosphere by the upward flux entering from the troposphere and deviating equatorward, particularly in August. However, in the upper stratosphere, a clear downward Eliassen-Palm flux is found below the eastward forcing center. Above the center, the Eliassen-Palm flux is upward. This shows that the forcing center is a generation region of Rossby waves with westward intrinsic phase speeds. Figures 4b, 4e, and 4h show the monthly averaged meridional gradient of potential vorticity. They exhibit an inversion of the meridional gradient at the top layers in June–July. A weak region of meridional gradient of potential vorticity extends downward and poleward from the inversion found in the top layers. The three winter months (June-July-August) present a negative meridional gradient at the pole between 50 and 5 hPa. To examine whether extra regions of negative meridional gradient appear along the month which are not dominant in the monthly mean, we count the number of days in the month for which an inversion of meridional gradient arises (right panels of Figure 4). The same region around the pole again manifests itself with more than 10 events in a month. In the equatorward flank of the jet, an inversion of potential vorticity meridional gradient events arises around 30°S with more than five events in each month. Note that there is no manifestation of these inversions of potential vorticity meridional gradient in the monthly mean in these latitudes.

We focus our attention on the time series of the forcing exerted by the Rossby wave components at the height of 1 hPa and in the latitudinal band from 65° to 75°S, which is one of the preferential regions of wave generation. The time series of the total EPFD is shown in Figure 5a (continuous line), we compare it with the EPFD that is contributed by the spectral band of 1.25–5.5 day periods and 1–3 wave numbers (dashed line). From May to mid-August, the total EPFD is eastward, and the filtered EPFD is able to account partially for the positive forcing. There is a difference of about 3 m s^{-1} d^{-1} that is expected to be contributed by waves outside the considered spectral band. As mentioned, our main hypothesis is that higher- and lower-frequency 1–5 wave number waves must be responsible for this contribution (Figure 2). On the other hand, after mid-August the total EPFD changes to westward. This change is expected to be produced by low-frequency Rossby waves that are propagating from the troposphere and breaking in the upper stratosphere at altitudes (zonal winds) where these waves are expected to have westward intrinsic phase speed. At this time of the year the stratosphere is preconditioned so that Rossby waves can penetrate along the wave guide up to these heights. Even when the total EPFD is westward from mid-August, showing that Rossby wave dissipation prevails at this time, the 1.25–5.5 day spectral band still presents an eastward forcing up to mid-September. In other words, the local Rossby wave generation events continue in this period, but they are not dominant.

Figure 5b shows the contribution of the different terms to the transformed Eulerian mean zonal wind equation, (7), at 1.0 hPa in MERRA reanalysis. During the instability period at this height, the westward forcing produced by gravity waves $\overline{X}_{GW}$ (dashed line in Figure 5b) of about −7 m s^{-1} d^{-1} is dominant. We incorporated in $\overline{X}_{GW}$ the forcing from orographic and nonorographic gravity wave parameterizations available in MERRA reanalysis data but also the zonal-mean zonal wind increments so this field includes the corrections produced by observations to the gravity wave momentum forcing [see *Scheffler and Pulido*, 2017]. The EPFD in MERRA reanalysis (continuous line in Figure 5a) is eastward with an average magnitude of 5 m s^{-1} d^{-1}. The Coriolis term (dotted line) balances the difference in magnitude between the two forcings, $\overline{X} + \overline{X}_{GW}$. It is about 2 m s^{-1} d^{-1} during the main period of local Rossby wave generation, from May to mid-August. The zonal mean acceleration term responds to short-term perturbations with a magnitude of about 1 m s^{-1} d^{-1}. After mid-August when low-frequency Rossby waves propagate from the troposphere up to this height and break there, the wave forcing drives the strong poleward meridional circulation seen in Figure 5b, so that one expects a strong descending motion in the polar region (not shown) which warms the pole and produces the final warming. Note also a slight increase in the gravity wave forcing which is also contributing to the vortex breakdown [*Scheffler and Pulido*, 2015]. Figure 5b shows the calculation of the gravity wave forcing (gray line) as a residual of the other three terms in (7) ($\overline{X}_{GW}$), and also from the forcing term from orographic and nonorographic gravity wave parameterizations and analysis increments which are available in

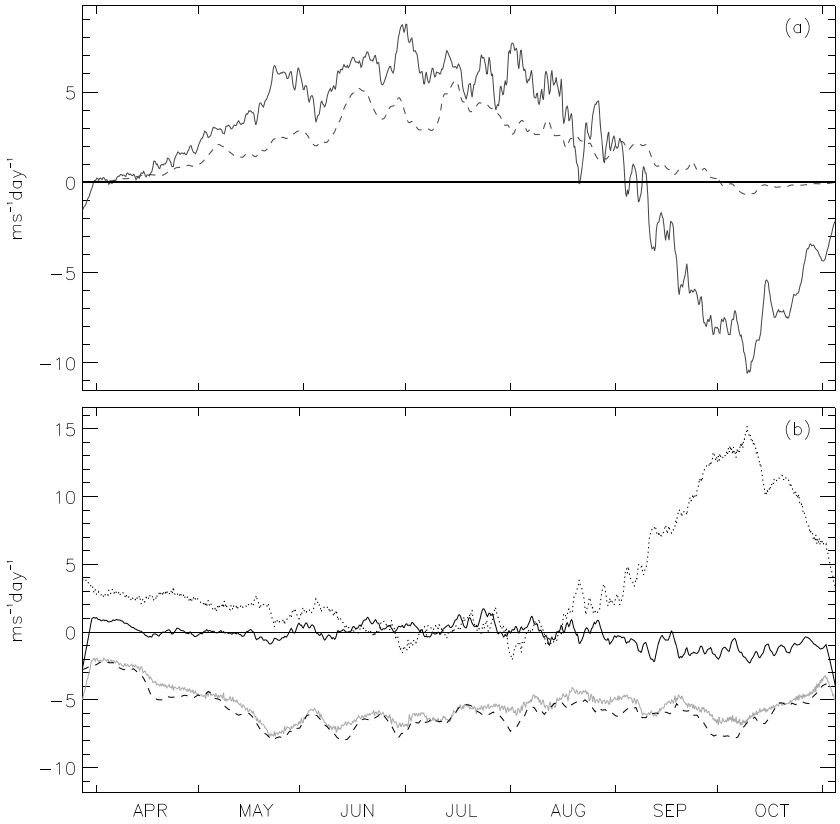

Figure 5. (a) Time series of the total EPFD (continuous line) at 1.0 hPa averaged in the latitudinal band from 65° to 75°S and averaged in the examined 20 years. EPFD corresponding to the 1.25–5.5 day period 1–3 zonal wave number spectral band (dashed line). (b) Time series of the contribution of the different terms of the transformed Eulerian mean zonal wind equation, zonal acceleration (continuous line), Coriolis term (dotted line), X_{GW} from the residual (gray line), and gravity wave drag from MERRA reanalysis (dashed line).

MERRA reanalysis (dashed line). Since these two terms are rather close, the transformed Eulerian mean analysis appears to be robust.

3.2. Two Case Studies

The large variability in terms of location, shape, and spatial distribution of the instability events does not allow us to produce clean composites of the events. We have therefore chosen two paradigmatic instability events to show in detail the main characteristics of the Rossby wave generation in MERRA reanalysis. The first case is a wave generation event that occurred in the poleward flank of the stratospheric jet during 11 to 15 July 2008. Figure 6 (left) shows a large eastward EPFD region between 50° and 80°S mainly located around 1 hPa, with two upward branches. The maximum eastward forcing exceeds 16 m s^{-1} d^{-1} in the inner contour. The zonal-mean zonal wind is also shown in Figure 6 (left). The event corresponds to a situation with double jet and the wave generation is located at the bottom of the secondary jet and between the two jets. The main jet is very strong exceeding 120 m/s. The Eliassen-Palm flux vectors clearly diverge from the generation region, the upward ones point toward the pole, while the waves propagating downward are deviated equatorward. The ones pointing upward appear to be partially responsible for the deceleration center located close to the pole at the top. The downward ones also appear to be the responsible for three weak deceleration centers located below the positive center. The critical surface for waves with wave number 2 and 2 day period represents a barrier for the downward propagating waves. Part of the region of eastward EPFD coincides with a sector where the meridional gradient of potential vorticity is negative (Figure 6, right), showing that the necessary conditions for baroclinic instability are satisfied. The regions are somewhat collocated; however, they do not coincide exactly, in particular, the eastward EPFD region is larger than the inversion of meridional gradient of potential vorticity region.

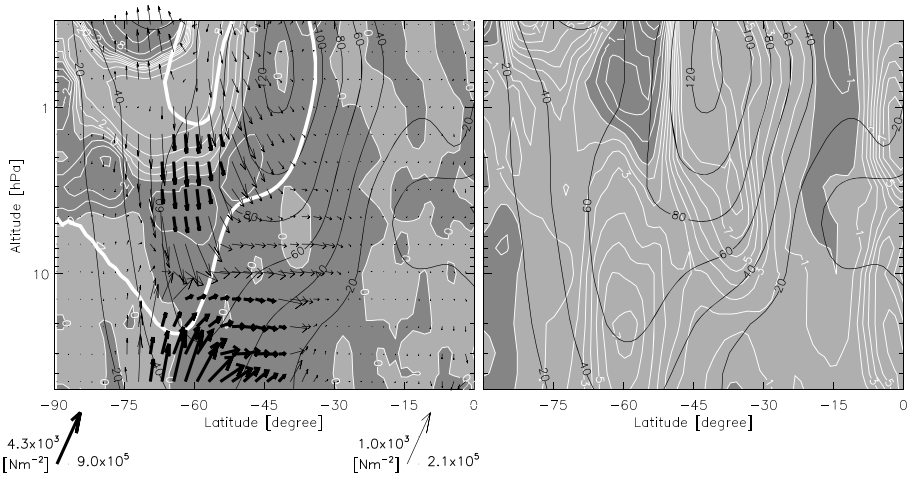

Figure 6. (left) EPFD during 11–15 July 2008 from perturbations filtered in the spectral band with periods of 1.25–5.5 days and wave numbers 1–3 (gray shading), the zonal-mean zonal wind (contours), and the Eliassen-Palm flux (vectors). The wide white curve indicates the critical surface for waves with wave number 2 and 2 day period. (right) Meridional gradient of potential vorticity (gray shading). The zonal-mean zonal wind is also shown for reference (contours). Note that vectors have two scales to make visible the Eliassen-Palm flux in the generation region.

The 4 day wave structure can be obtained with the analysis of the amplitude and phase of the wave event from the potential temperature field. The analysis follows the coherence procedure detailed in *Garcia et al.* [2005]. Figure 7 (top) shows the amplitude of the $s = 2$ wave from 28 June to 29 July 2008. The maximum amplitude of the wave event is found at about 1 hPa and 60°S. From the position of the peak amplitude, the phase increases downward (Figure 7, bottom). This means a heat flux equatorward, and it is coherent with the downward vertical component of the Eliassen-Palm flux found at that height in Figure 6 (left). From the position of the peak amplitude, the phase also increases equatorward in coherence with the equatorward Eliassen-Palm flux found there. Poleward of the peak amplitude, there is a negligible phase change in latitude but not in altitude. We note that the Rossby wave event propagates eastward at a ground-based phase speed of around 40 m s^{-1}; however, the event possesses a westward intrinsic phase speed.

The wave generation events that occur in the equatorward flank of the jet are more sporadic than poleward flank ones. In general, they are found in September when the polar vortex is located at higher latitudes and the core is descending. We chose one event that occurred between 1 and 5 September 1992. Three positive EPFD centers are found (Figure 8, left): one at the pole flank of the jet at about 0.5 hPa, one at the equatorward flank of the jet at about 1 hPa, and one at the reanalysis top 0.1 hPa. The divergence of Eliassen-Palm flux vectors is evident at the equatorward flank of the jet. The critical surface for Rossby waves with wave number 2 and 4.5 day period is located close to the region of generation in the separation between the equatorward and poleward propagating waves. The Eliassen-Palm flux of the waves propagating equatorward appear to have a sink region located close to −30°S. At lower heights, a strong Eliassen-Palm flux is present at the jet core with a significant downward propagating component in the polar flank of the jet core (between 10 hPa and 2 hPa). Figure 8 (right) shows the meridional gradient of potential vorticity. Even when there is a strong positive EPFD center at 1 hPa at the equatorward flank of the jet, there is no signature of a potential vorticity gradient inversion there.

3.3. Climatological Characterization of the Events

We applied the automatic event detection technique to the 20 years of MERRA reanalysis to characterize statistically the wave generation events. Figure 9a shows the total number of wave generation events as a function of the month in the 20 years. They are concentrated mostly from June to September reaching a total number of 118 events in July (a mean of six events in July per year, and a similar value slightly lower for August). An average of four events occurs during June and September. The number of events registered in May is 50 (average of 2.5 events during the month). The interannual variability of the number of events is shown in Figure 9b. The number of events in the austral spring months depends on the strength of the jet and the date of the final warming. For years with late vortex breakdown, a relatively large number of cases is registered in October. The dispersion of the number of events in July, for instance, is quite large. There are years with

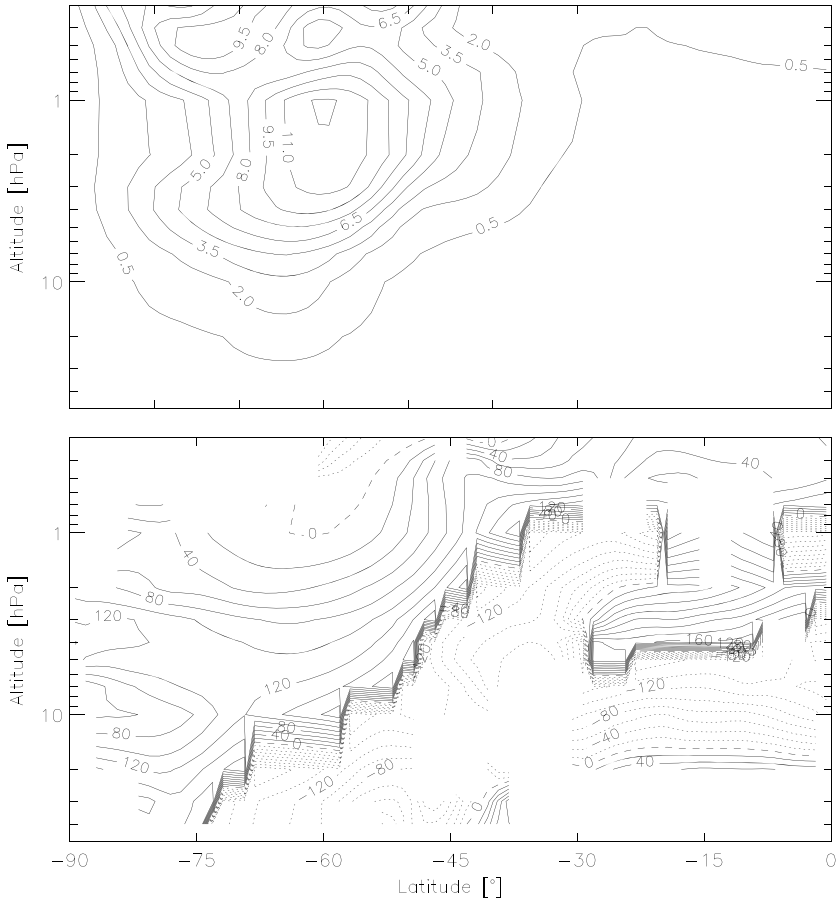

Figure 7. (top) Amplitude and (bottom) phase structure for the $s = 2$ wave from the potential temperature for the period 28 June to 29 July 2008.

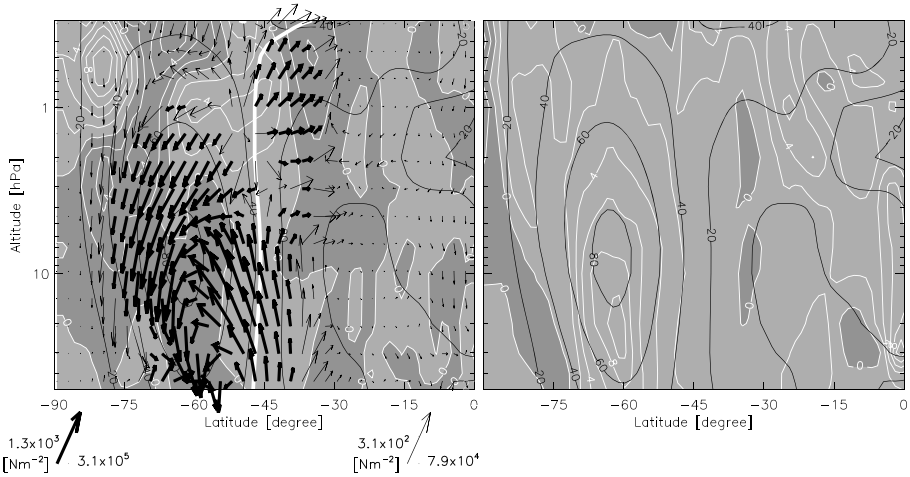

Figure 8. (left) EPFD averaged during 1–5 September 1992 contributed by the spectral band with periods of 1.25–5.5 days and wave numbers 1–3 (light shading represents positive EPFD), the zonal-mean zonal wind (contours), and the Eliassen-Palm flux (vectors). The wide black curve indicates the critical surface for waves with wave number 2 and 4.5 day period. (right) Meridional gradient of potential vorticity (dark gray shading represents negative meridional gradient). The zonal-mean zonal wind is also shown for reference (contours). Note that vectors have two scales.

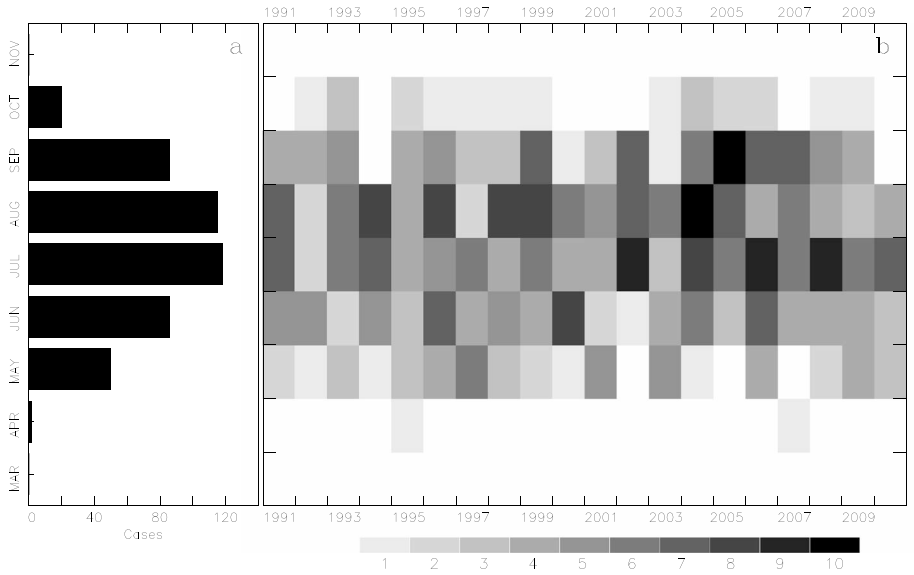

Figure 9. (a) Total number of Rossby wave generation cases registered along the 20 years as a function of month. (b) Number of events as a function of the year and month.

two events in July and others with 10 events. During the year of the southern sudden stratospheric warming, 2002, no case was detected in May, a very few cases were detected in June, but then a large number of cases occurred in July. Indeed, this month had 10 events, one of the largest monthly totals recorded in the 20 years analyzed. August and September of that year were also particularly active months in terms of wave generation (seven detected events in each month).

As already mentioned, the detection algorithm also tracks the events in different time frames. The duration of the events can then be measured. We then classified in a histogram the number of events as a function of the duration. Figure 10 shows the probability distribution; it clearly follows an exponential distribution. The characteristic time (mean of the exponential distribution) is 3.35 days. Although most of the cases have a duration shorter than 5 days, there are a few very long events which last for 10 days and even more. Of course, this statistic may change if we change the detection criteria. In particular, for the long-duration events, more strict thresholds will increase the number of cases and diminish the length. However, their appearance does indicate in a few cases that a rather localized region remains with unstable conditions and eastward EPFD for several days.

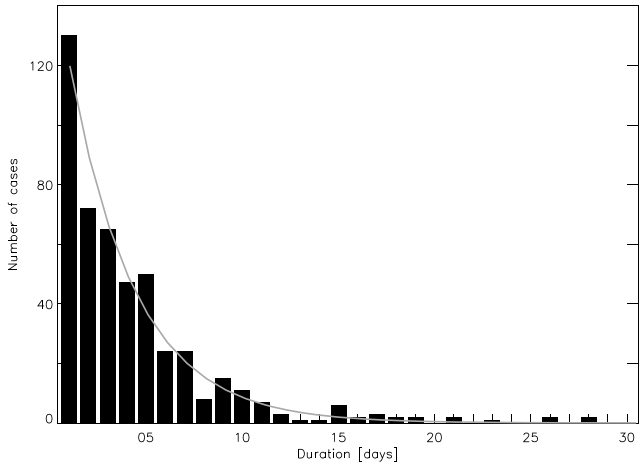

Figure 10. Histogram of the number of events of Rossby wave generation as a function of the duration of the events for the 20 years. The fitted exponential distribution is shown.

Figure 11a shows the distribution of events as a function of height. As already mentioned, the preferential height of the instability center is 0.7 hPa with a very large number of cases (190). This is indeed the height chosen for specific fixed altitude analyses. At this height at least two latitudes show a large number of cases, latitudes poleward of −80° and around −60°S (Figure 11b). The cases centered at 60°S should not be associated with Rossby wave generation in the equatorward flank of the jet. They are at least partially due to a double-jet structure and also a jet located in midlatitudes as found in June (see, for instance, the case study shown in Figure 6). The V-shaped pattern found in Figure 11b is a manifestation of generation along the region between

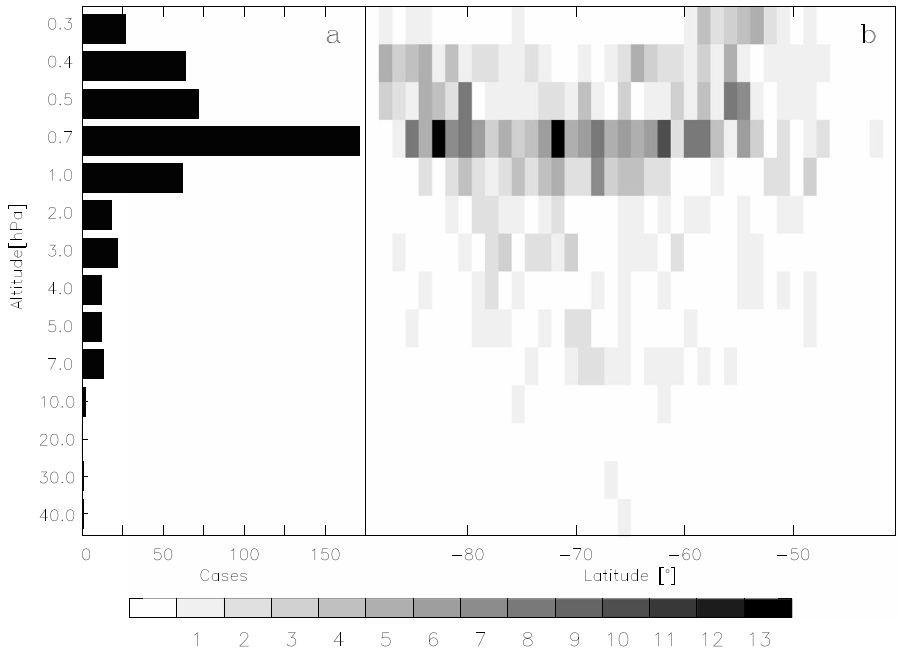

Figure 11. Number of Rossby wave generation events (a) as a function of height and (b) as a function of height and latitude.

the two jets and poleward of them. The events can be found also at lower heights as low as 10 hPa, one was located at 40 hPa and 66°S. The statistics above 0.7 hPa, close to the top of the MERRA model, 0.01 hPa, may be affected by the presence of the sponge layer.

To examine the spectral characteristics of the generated waves in the detected events, we determine the dominant frequency and zonal wave number of the generated waves using Fourier analysis. We conducted a Fourier analysis for each detected event. A Hanning window is applied to the time series with a width of 16 days centered at the date of the event (time frame of maximum amplitude); in this way the wave events are isolated. A 2-D Fourier transform, in time and in longitude, is then applied to the fields. The resulting maximal frequency-wave number spectral densities are used to classify the events. The probabilistic distribution as a function of the adimensional zonal wave number times the period, $s \times \tau$, are shown in Figure 12. The probability distribution is quite remarkably peaked at $k \times \tau = (3.78 \pm 0.02)$ days with a width of (0.71 ± 0.02) day showing that the eastward forcing events are associated with the so-called 4 day waves generated in the middle atmosphere. A number of cases are detected with $s \times \tau$ greater than 7 days so that a Gamma distribution would fit better the histogram. The dispersion found around the peak corresponds to the spectral distribution

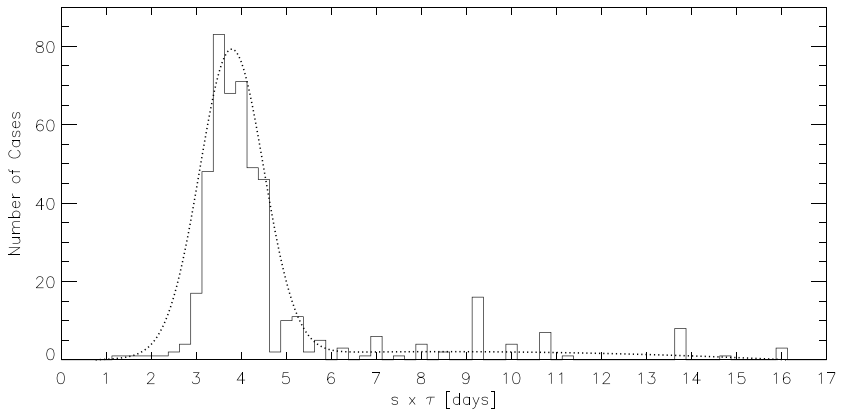

Figure 12. Histogram of the number of events of Rossby wave generation as a function of the zonal wave number times the period, $s \times \tau$. The fitted Gaussian distribution is shown for reference.

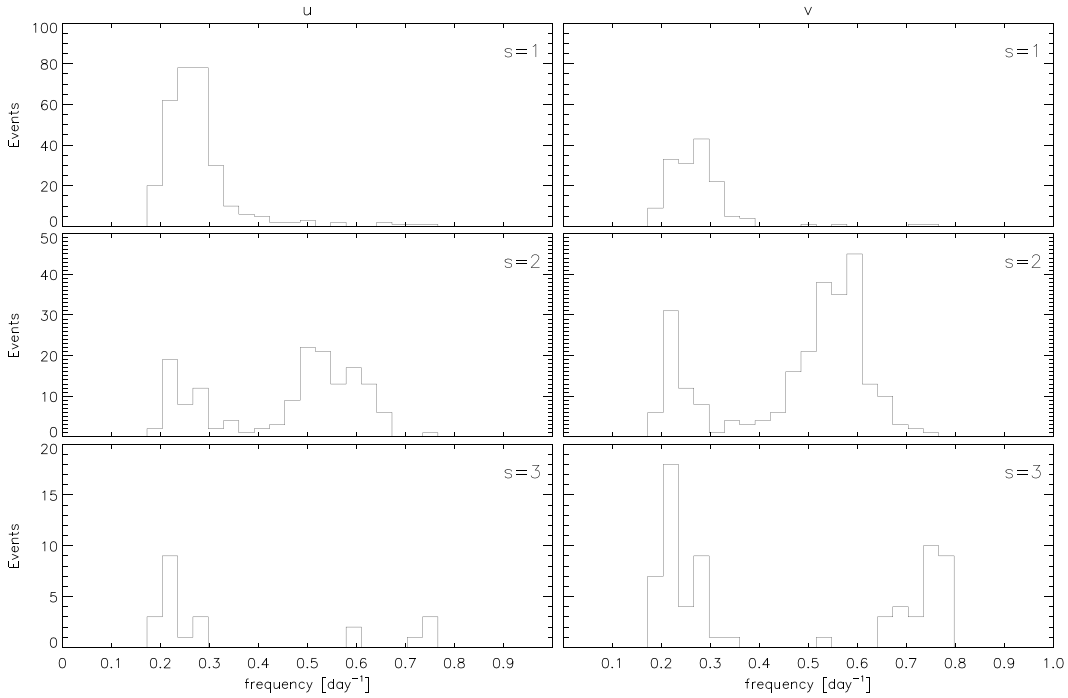

Figure 13. Histogram of the number of events of Rossby wave generation as a function of the frequency of the events. (left column) Zonal wind perturbation. (right column) Meridional wind perturbation.

found in the power spectrum density around the expected frequencies of the unstable barotropic-baroclinic modes (see Figure 2).

Figure 13 shows the number of events as a function of frequency at a fixed zonal wave number. For $s=1$, the zonal and meridional wind perturbations show a peak around 0.25 day^{-1}. For $s=2$ and $s=3$, they exhibit bimodal distributions, one peak at about 0.2 day^{-1} which is indeed dominant for $s=3$. For $s=2$, the other peak is found at 0.55 day^{-1} and for $s=3$ at 0.75 day^{-1}. The last peak is more visible in the meridional wind perturbation (Figure 13, right column). This is expected since meridional wind perturbations in Rossby waves are larger for larger wave number. The 4 day events are not monochromatic; they are like large-scale pools so that several Fourier modes contribute to shape these patterns. The secondary peaks have a fixed frequency wave number ratio so that they occur for a fixed phase speed.

4. Conclusions

The middle atmosphere exhibits a high internal variability during winter. A rich frequency spectrum of large-scale Rossby waves is internally generated through barotropic-baroclinic instabilities. A divergent Eliassen-Palm momentum flux is found in the generation regions. This is associated with downward and upward propagating waves. However, the amplitude of upward waves is, in general, larger because of the decrease of density with height. Although we called them wave generation events, it may also be the case that they are enhancement events in which certain existing modes are reinforced by the instability. The eastward forcing associated with the divergent Eliassen-Palm momentum flux dominates the austral winter stratopause even for the 20 year monthly mean fields in the MERRA data examined, with a maximum of 7 m s^{-1} d^{-1} in July.

The concomitant westward forcing produced by the breaking of the internally generated Rossby waves, which propagate upward, is produced just above the generation location toward the pole. It involves a significant monthly averaged zonal-mean westward forcing that exceeds 10 m s^{-1} d^{-1} for waves with 1.25–5.5 day period and 1–3 wave numbers. A smaller westward forcing to the general circulation is produced by the downward propagating waves, but it is still clearly visible at least in the examined case studies. To put it in more general terms, although the net effect of these internally generated Rossby waves in the whole middle atmosphere is null, they play a very important role *redistributing momentum vertically*.

The zonal-mean budget analysis in the transformed Eulerian mean framework at 1.0 hPa shows that the eastward EPFD in high latitudes is balanced by gravity wave drag which is rather similar to the residual term in the transformed Eulerian mean zonal wind equation. However, the main role of gravity waves is expected to be a deceleration of the middle atmosphere jet and closing of the jet [*Pulido and Thuburn*, 2008].

The Rossby wave generation produces a significant redistribution of momentum in the vertical which has an important impact on the general circulation so that general circulation models need to reproduce the local generation to give a realistic evolution of the southern polar vortex. The deceleration produced by the internally generated Rossby waves propagating upward contributes to the closing of the jet in the polar region above 1 hPa. The westward forcing produced by the upward components at those heights exceeds 10 m s^{-1} d^{-1} so that these waves play a major role in the momentum budget of the lower mesosphere. The forcing magnitude is similar to the forcing produced by gravity waves at those heights [*Alexander and Rosenlof*, 1996; *Alexander et al.*, 2010; *Pulido and Thuburn*, 2008]. The strong middle atmosphere jet and the presence of the double-jet structure during austral winter establish more favorable conditions for internally generated Rossby waves and are expected to be of larger magnitude than during boreal winter [*Lawrence and Randel*, 1996; *Watanabe et al.*, 2009].

The generated Rossby waves are expected to be an important climatological behavior of the upper mesosphere and lower thermosphere. Regrettably, MERRA reanalysis does not allow us to examine the whole impact of the upward propagating waves, since it is constrained to altitudes lower than 0.1 hPa. These waves are expected to interact with other dynamical features present in the mesosphere and the lower thermosphere. *McCormack et al.* [2009] have found that the strong planetary forcing in the boreal winter that led to a SSW in 2006 played an important role, through the pole-to-pole residual meridional circulation in the upper middle atmosphere, in modulating the 2 day wave observed in the austral summer. *Chandran et al.* [2013] reported secondary planetary waves in the mesosphere and the lower thermosphere, which were generated following a stratospheric sudden warming in January 2002. *Sassi and Liu* [2014] showed that upward propagating planetary waves to the lower thermosphere of wave numbers 1 and 2 and periods between 2 and 10 days are deflected toward the tropics influencing the amplitude of equatorially trapped waves.

The maximum number of Rossby wave generation events is detected in July and August, but they are found up to September and a few in October during the vortex breakdown. On average, six events are detected in the most active months—July and August. The duration of the events follows an exponential distribution with a characteristic time of 3.35 days. The center of the events is located in a latitudinal band, between 60° to 80°S and a maximum number of events is found at 0.7 hPa. However, they may be located as low as 7 hPa during the jet descent in September–October. On average, there are 24 events per year.

A clear monthly mean eastward EPFD center is found in the equatorward flank of the jet. We did not find a signature of inversions located at the equatorward flank of the jet in the monthly mean potential vorticity meridional gradient. However, daily potential vorticity meridional gradient fields manifest more than five inversion events in a month in the equatorward flank of the jet during the austral winter months.

Acknowledgments
The authors thank two anonymous reviewers for helpful and pertinent comments. This work was partially supported by a PIP 112-20120100414CO grant from CONICET and PICT2015-2368 grant from ANPCYT (Argentina). It also benefited from the use of computational facilities at CECONEA (UNNE). MERRA data have been provided by the Global Modeling and Assimilation Office (GMAO) at NASA Goddard Space Flight Center through the NASA GES DISC online archive (via http://disc.sci.gsfc.nasa.gov).

References

Alexander, M. J., and K. H. Rosenlof (1996), Nonstationary gravity wave forcing of the stratospheric zonal mean wind, *J. Geophys. Res.*, *101*, 23465–23474.

Alexander, M. J., et al. (2010), Recent developments in gravity wave effects in climate models and the global distribution of gravity wave momentum flux from observations and models, *Q. J. R. Meteorol. Soc.*, *136*, 1103–1124.

Andrews, D. G., and M. E. McIntyre (1978), On wave-action and its relatives, *J. Fluid Mech.*, *89*, 647–664, doi:10.1017/S0022112078002785.

Andrews, D. G., J. R. Holton, and C. B. Leovy (1987), *Middle Atmosphere Dynamics*, Academic Press, San Diego, Calif.

Butchart, N. (2014), The Brewer-Dobson circulation, *Rev. Geophys.*, *52*, 157–184, doi:10.1002/2013RG000448.

Chandran, A., R. R. Garcia, R. L. Collins, and L. C. Chang (2013), Secondary planetary waves in the middle and upper atmosphere following the stratospheric sudden warming event of January 2012, *Geophys. Res. Lett.*, *40*, 1861–1867, doi:10.1002/grl.50373.

Charney, J., and P. G. Drazin (1961), Propagation of planetary-scale disturbances from the lower into the upper atmosphere, *J. Geophys. Res.*, *66*, 83–109.

Charney, J., and M. E. Stern (1962), On the stability of internal baroclinic jets in a rotating atmosphere, *J. Atmos. Sci.*, *19*, 159–172.

Coy, L., I. Štajner, A. M. DaSilva, J. Joiner, R. B. Rood, S. Pawson, and S. J. Lin (2003), High-frequency planetary waves in the polar middle atmosphere as seen in a data assimilation system, *J. Atmos. Sci.*, *60*, 2975–2992, doi:10.1175/1520-0469(2003)060.

Garcia, R. R. (1987), On the mean meridional circulation of the middle atmosphere, *J. Atmos. Sci.*, *44*, 3599–3609.

Garcia, R. R., R. Lieberman, J. M. Russel III, and M. G. Mlynczak (2005), Large-scale waves in the mesosphere and lower thermosphere observed by SABER, *J. Atmos. Sci.*, *62*, 4384–4399.

Hartmann, D. L. (1983), Barotropic instability of polar night jet stream, *J. Atmos. Sci.*, *40*, 817–835.

Lawrence, B. N., and W. J. Randel (1996), Variability in the mesosphere observed by the Nimbus 6 pressure modulator radiometer, *J. Geophys. Res.*, *101*, 23,475–23,489.
Lawrence, B. N., G. J. Fraser, R. A. Vincent, and A. Phillips (1995), The 4-day wave in the Antarctic mesosphere, *J. Geophys. Res.*, *100*, 18,899–18,908.
Lu, X., X. Chu, T. Fuller-Rowell, L. Chang, W. Fong, and Z. Yu (2013), Eastward propagating planetary waves with periods of 1–5 days in the winter Antarctic stratosphere as revealed by MERRA and lidar, *J. Geophys. Res. Atmos.*, *118*, 9565–9578, doi:10.1002/jgrd.50717.
Manney, G. L. (1991), The stratospheric 4-day wave in NMC data, *J. Atmos. Sci.*, *48*, 1798–1811.
Manney, G. L., and W. J. Randel (1993), Instability at the winter stratopause: A mechanism for the 4-day wave, *J. Atmos. Sci.*, *50*, 3928–2928.
McCormack, J. P., L. Coy, and K. W. Hoppel (2009), Evolution of the quasi 2-day wave during January 2006, *J. Geophys. Res.*, *114*, D20115, doi:10.1029/2009JD012239.
Nezlin, Y., YJ Rochon, and S Polavarapu (2009), Impact of tropospheric and stratospheric data assimilation on mesospheric prediction, *Tellus*, *61A*, 154–159.
Polavarapu, S., and M. Pulido (2017), Stratospheric and mesospheric data assimilation: The role of middle atmospheric dynamics, in *Data Assimilation for Atmospheric, Oceanic and Hydrologic Applications*, vol. III, pp. 429–454, Springer, New York, doi:0.1007/978-3-319-43415-5_19.
Prata, A. J. (1984), The 4-day wave, *J. Atmos. Sci.*, *41*, 150–155.
Pulido, M. (2014), A simple technique to infer the missing gravity wave drag in the middle atmosphere using a general circulation model: Potential vorticity budget, *J. Atmos. Sci.*, *71*, 683–697.
Pulido, M., and J. Thuburn (2006), Gravity wave drag estimation from global analyses using variational data assimilation principles. II: A case study, *Q. J. R. Meteorol. Soc.*, *132*, 1527–1543, doi:10.1256/qj.05.43.
Pulido, M., and J. Thuburn (2008), The seasonal cycle of gravity wave drag in the middle atmosphere, *J. Clim.*, *21*, 4664–4679.
Rienecker, M. M., et al. (2011), MERRA: NASA's Modern-Era Retrospective Analysis for Research and Applications, *J. Clim.*, *24*, 3624–3648, doi:10.1175/JCLI-D-11-00015.1.
Sassi, F., and H. L. Liu (2014), Westward traveling planetary wave events in the lower thermosphere during solar minimum conditions simulated by SD-WACCM-X, *J. Atmos. Sol. Terr. Phys.*, *119*, 11–26.
Scavuzzo, C. M., M. A. Lamfri, H. Teitelbaum, and F. Lott (1998), A study of the low-frequency inertio-gravity waves observed during the Pyrénées experiment, *J. Geophys. Res.*, *103*, 1747–1758, doi:10.1029/97JD02308.
Scheffler, G., and M. Pulido (2015), Compensation between resolved and unresolved wave drag in the stratospheric final warmings of the Southern Hemisphere, *J. Atmos. Sci.*, *72*, 4393–4411, doi:10.1175/JAS-D-14-0270.1.
Scheffler, G., and M. Pulido (2017), Estimation of gravity-wave parameters to alleviate the delay in the Antarctic vortex breakup in general circulation models, *Q. J. R. Meteorol. Soc.*, *143*, 2157–2167, doi:10.1002/qj.3074.
Venne, D. E., and J. L. Stanford (1979), Observations of a 4-day temperature wave in the polar winter stratosphere, *J. Atmos. Sci.*, *36*, 2016–2019.
Watanabe, S., Y. Tomikawa, K. Sato, Y. Kawatani, K. Miyazaki, and M. Takahashi (2009), Simulation of the eastward 4-day wave in the Antarctic winter mesosphere using a gravity wave resolving general circulation model, *J. Geophys. Res.*, *114*, D16111, doi:10.1029/2008JD011636.